J|A|C|S
ARTICLES
Published on Web 03/03/2007

Continuous Structural Evolution of Calcium Carbonate Particles: A Unifying Model of Copolymer-Mediated Crystallization

Alex N. Kulak,[†] Peter Iddon,[‡] Yuting Li,[‡] Steven P. Armes,[‡] Helmut Cölfen,*[,§] Oskar Paris,[§] Rory M. Wilson,[||] and Fiona C. Meldrum*[,†]

Contribution from the School of Chemistry, University of Bristol, Cantock's Close, Bristol, BS8 1TS, United Kingdom, Department of Chemistry, University of Sheffield, Brook Hill, Sheffield S3 7HF, United Kingdom, Max Planck Institute of Colloids and Interfaces, Colloid Chemistry and Biomaterials Department, Research Campus Golm, Am Mühlenberg, D-14424 Potsdam, Germany, and Materials Department, Queen Mary, University of London, Mile End Road, London E1 4NS, United Kingdom

Received October 25, 2006; E-mail: fiona.meldrum@bristol.ac.uk; coelfen@mpikg.mpg.de

Abstract: Two double-hydrophilic block copolymers, each comprising a nonionic block and an anionic block comprising pendent aromatic sulfonate groups, were used as additives to modify the crystallization of $CaCO_3$. Marked morphological changes in the $CaCO_3$ particles were observed depending on the reaction conditions used. A poly(ethylene oxide)-*b*-poly(sodium 4-styrenesulfonate) diblock copolymer was particularly versatile in effecting a morphological change in calcite particles, and a continuous structural transition in the product particles from polycrystalline to mesocrystal to single crystal was observed with variation in the calcium concentration. The existence of this structural sequence provides unique insight into the mechanism of polymer-mediated crystallization. We propose that it reflects continuity in the crystallization mechanism itself, spanning the limits from nonoriented aggregation of nanoparticles to classical ion-by-ion growth. The various pathways to polycrystalline, mesocrystal, and single-crystal particles, which had previously been considered to be distinct, therefore all form part of a unifying crystallization framework based on the aggregation of precursor subunits.

Introduction

Block copolymers have been demonstrated to be effective crystal growth modifiers, producing homogeneous populations of particles frequently with unusual morphologies.[1−3] Part of the attraction of using copolymers to modulate crystallization processes derives from their versatility. The scope for tuning the copolymer structure is enormous, and it is well known that subtle changes, for example, in the relative block lengths, can lead to significant changes in the particle morphology.[1−3] Further, variation of the composition and pH of the crystallizing solution can change the mode of interaction between the developing particles and the copolymer chains, resulting in large morphological effects.

In investigating the use of block copolymers as crystal growth additives, calcium carbonate has received considerable attention. Calcium carbonate is an industrially important material in applications such as fillers and coatings. It offers an attractive test material as it is polymorphic, exhibiting three anhydrous polymorphs, calcite aragonite, and vaterite,[4] and simple additives are known to be effective in producing a range of morphologies.[5−7] A wide range of copolymers, typically comprising a nonionic block and an ionic block bearing side groups such as carboxylates, sulfonates, and phosphates,[8] have been shown to mediate formation of calcite particles with morphologies including hollow spheres,[9] spherules,[10] and dumbbells.[11] Stabilization of vaterite structures can also be achieved to produce particles such as disks,[9] flowers,[12] and hollow spheres,[13] depending on the precise structure of the copolymer. All of these particles have been reported to be nonoriented, polycrystalline aggregates.

Precipitation of calcium carbonate in the presence of block copolymers typically begins with formation of precursor amorphous calcium carbonate (ACC) particles, which subsequently

[†] University of Bristol.
[‡] University of Sheffield.
[§] Max Planck Institute of Colloids and Interfaces, Colloid Chemistry (H.C.) and Biomaterials Department (O.P.).
[||] University of London.

(1) Yu, S. H.; Cölfen, H. *J. Mater. Chem.* **2004**, *14*, 2124−2147.
(2) Yu, S.-H.; Cölfen, H.; Antonietti, M. *J. Phys. Chem. B* **2003**, *107*, 7396−7405.
(3) Robinson, K. L.; Weaver, J. V. M.; Armes, S. P.; Diaz-Marti, E.; Meldrum, F. C. *J. Mater. Chem.* **2002**, *12*, 890−896.
(4) Meldrum, F. C. *Int. Mater. Rev.* **2003**, *48*, 187−224.
(5) Mann, S.; Didymus, J. M.; Sanderson, N. P.; Heywood, B. R.; Sumper, E. J. A. *J. Chem. Soc., Faraday Trans.* **1990**, *86*, 1873−1880.
(6) Tong, H.; Ma, W.; Wang, L.; Wan, P.; Hu, J.; Cao, L. *Biomaterials* **2004**, *25*, 3923−3929.
(7) Wei, H.; Shen, Q.; Zhao, Y.; Zhou, Y.; Wang, D.; Xu, D. *J. Cryst. Growth* **2005**, *279*, 439−446.
(8) Cölfen, H. *Macromol. Rapid Commun.* **2001**, *22*, 219−252.
(9) Qi, L.; Li, K.; Ma, J. *Adv. Mater.* **2002**, *14*, 300−303.
(10) Yu, S. H.; Cölfen, H.; Hartmann, J.; Antonietti, M. *Adv. Funct. Mater.* **2002**, *12*, 541−545.
(11) Cölfen, H.; Qi, L. *Chem. Eur. J.* **2001**, *7*, 106−116.
(12) Rudloff, J.; Antonietti, M.; Colfen, H.; Pretula, J.; Kaluzynski, K.; Panczek, S. *Macromol. Chem. Phys.* **2002**, *203*, 627−635.
(13) Cölfen, H.; Antonietti, M. *Langmuir* **1998**, *14*, 582−589.

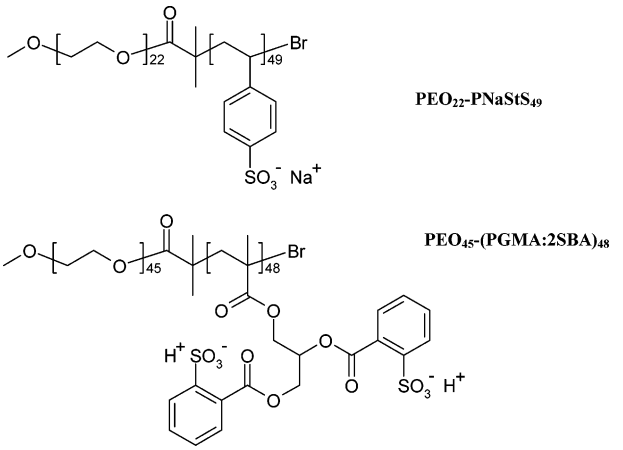

Figure 1. Chemical structures of the two sulfonated water-soluble diblock copolymers PEO_{22}-$PNaStS_{49}$ and PEO_{45}-$(PGMA:2SBA)_{48}$.

transform into either vaterite or calcite primary particles. Temporary stabilization of these primary units by interaction with the block copolymers retards further growth such that aggregation of these particles proceeds more rapidly than growth of individual particles, resulting in formation of polycrystalline particles.[1] A particular feature of copolymer-mediated precipitation is the potential for oriented aggregation of primary particles. This has been observed in a wide range of systems, including formation of $BaCrO_4$[14] and $BaSO_4$ fibers and fiber bundles.[15] Formation of $CaCO_3$ particles based on oriented aggregation appears to be less common, but needle-like calcite particles generated using an acrylate−styrene copolymer[16] and two-dimensional vaterite platelet assembles,[17] both of which diffract as single crystals, have been reported. Recent observations by Cölfen and co-workers have also shown that poly(sodium 4-styrenesulfonate) can direct formation of a category of calcite particles christened "mesocrystals".[18−21] These particles had sizes and morphologies that were consistent with single crystals of calcite, and examination between crossed polars in an optical microscope demonstrated uniform extinction as is characteristic of single crystals. Conversely, their high surface roughness and large surface areas were more consistent with a polycrystalline structure.

In this paper we compare the influence of two diblock copolymers, each comprising a nonionic poly(ethylene oxide) (PEO) block and an anionic block comprising pendent aromatic sulfonate groups (see Figure 1), on the precipitation of calcium carbonate. Interestingly, although displaying marked similarities in structure, these polymers behave quite differently in their ability to control the morphologies of calcium carbonate particles. While the PEO_{45}-$(PGMA:2SBA)_{48}$ diblock copolymer only produces particles with morphologies that are consistent with 'single-crystal'-type particles, the PEO_{22}-$PNaStS_{49}$ diblock copolymer mediates the growth of particles with microstructures ranging from polycrystalline aggregates to oriented "mesocrystals" to single crystals depending on the precise synthesis conditions. Moreover, a continuous morphological and structural transition between these crystals can be observed, offering considerable insight into the mechanism of formation of calcium carbonate particles in the presence of diblock copolymers. This structural transition was investigated using microbeam diffraction to interrogate members of the morphological sequence, demonstrating a degree of orientational ordering even in the polycrystalline particles.

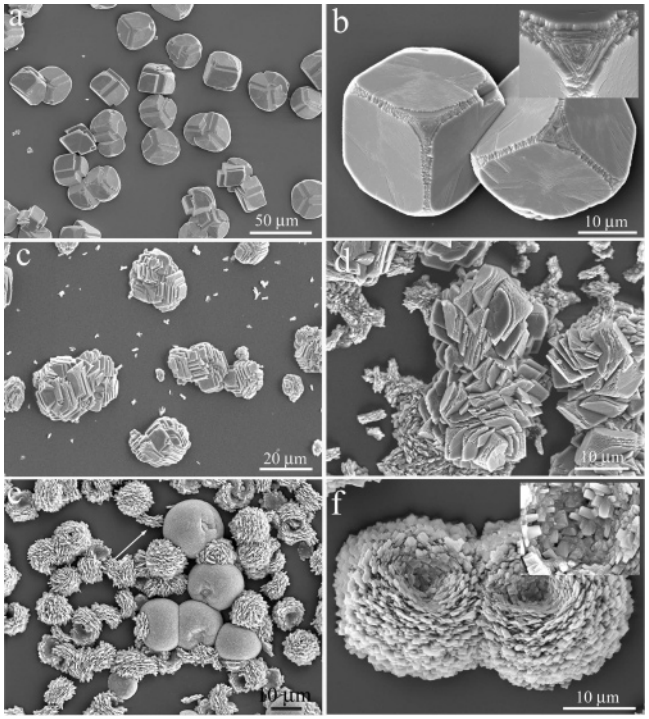

Figure 2. Calcium carbonate crystals precipitated from a solution containing 10 mM Ca and PEO_{22}-$PNaStS_{49}$ at a concentration such that the [Ca]:[S] molar ratio (where [S] is the molar concentration of polymerized sulfonate groups) was (a) 250:1, (b) 250:1, (c) 125:1, (d) 20:1, (e) 12.5:1, and (f) 12.5:1.

Results

A marked dependence of the crystal morphology on the [Ca]:[S] molar ratio was observed for the PEO_{22}-$PNaStS_{49}$ copolymer (Figure 2). For [Ca] = 10 mM, low [Ca]:[S] molar ratios of 250:1 yielded calcite particles 20−30 μm in size with modified rhombohedral morphologies (Figure 2a and 2b). Confirmation of the assignment of calcite was made by both Raman microscopy studies on individual particles and also XRD of the entire sample, which corresponded to 100% calcite. A typical Raman spectrum of a calcite particle is shown in the Supporting Information (SI), Figure 1a. The 1087 cm^{-1} vibration corresponds to the internal υ_1 vibration, the 714 cm^{-1} band to the internal υ_4 vibration, and the 284 cm^{-1} feature to a lattice vibration.[22] The corners and edges of the rhombohedra were truncated, yielding eight new triangular faces and an overall rounded appearance. The population of crystals also showed a marked orientational effect with more than one-half of the particles oriented such that the [001] axis was perpendicular to

(14) Yu, S. H.; Cölfen, H.; Antonietti, M. *Chem. Eur. J.* **2002**, *8*, 2937−2945.
(15) Qi, L.; Cölfen, H.; Antonietti, M.; Li, M.; Hopwood, J. D.; Ashley, A. J.; Mann, S. *Chem. Eur. J.* **2001**, *7*, 3526−3532.
(16) Moore, L.; Hopwood, J. D.; Davey, R. J. *J. Cryst. Growth* **2004**, *261*, 93−98.
(17) Gehrke, N.; Cölfen, H.; Pinna, N.; Antonietti, M.; Nassif, N. *Cryst. Growth Des.* **2005**, *5*, 1317−1319.
(18) Wang, T. X.; Cölfen, H.; Antonietti, M. *J. Am. Chem. Soc.* **2005**, *127*, 3246−3247.
(19) Wohlrab, S.; Pinna, N.; Antonietti, M.; Cölfen, H. *Chem. Eur. J.* **2005**, *11*, 2903−2913.
(20) Cölfen, H.; Antonietti, M. *Angew. Chem., Int. Ed.* **2005**, *44*, 5576−5591.
(21) Wang, T. X.; Antonietti, M.; Cölfen, H. *Chem. Eur. J.* **2006**, *12*, 5722−5730.
(22) Behrens, G.; Kuhn, L. T.; Ubic, R.; Heuer, A. H. *Spectrosc. Lett.* **1995**, *28*, 983−995.

the substrate. This orientation was confirmed by the 3-fold symmetry of the top face of these particles and the observation of extinction when viewing these crystals between crossed polars in an optical microscope, indicating that they were viewed down the isotropic [001] axis. The crystal faces were quite smooth, although most showed evidence of minor roughening. Decreasing the [Ca]:[S] molar ratio to 125:1 produced calcite particles with irregular, intergrown morphologies (Figure 2c). Some evidence for truncation of the edges and corners of the calcite rhombohedra was found in these particles.

A [Ca]:[S] molar ratio of 20:1 produced two types of particles. The first had large, intergrown morphologies similar to those obtained at a [Ca]:[S] molar ratio of 125:1, and the second was a new type of polycrystalline aggregate (Figure 2d). The polycrystalline aggregates exhibited a layered structure and appeared either as $\sim$5 μm individual particles or larger aggregates. Both categories of particles were identified as calcite by Raman microscopy. A full transition to the polycrystalline particles was achieved for [Ca]:[S] molar ratios ranging from 1:3 to 12.5:1. At [Ca]:[S] = 12.5:1, a uniform population of polycrystalline aggregates of $\sim$12 μm diameter was produced (Figure 2e and 2f). These particles had a layered structure and typically displayed evidence of a hexagonal profile. Some variation in the particle thickness was observed, such that the top surfaces of thinner particles were quite flat (arrowed in Figure 2e), while continued build-up of layers generated thicker, more spherical particles with a central depression (Figure 2f). These particles were identified as calcite by Raman microscopy. In addition to these calcite particles, spherical vaterite particles of diameter $\approx$ 20 μm were also produced, as confirmed by Raman microscopy, and XRD of the entire sample showed a typical composition of 48% calcite and 52% vaterite. A representative Raman spectrum of a vaterite particle is shown in SI Figure 1b, where the split signal at 1091 cm^{-1} is characteristic of the internal υ_1 vibration, the band at 754 cm^{-1} is due to the internal υ_1 vibration, and the peak at 306 cm^{-1} is assigned to a lattice mode.[22] For [Ca]:[S] molar ratios ranging from 1:3 to 12.5:1, a higher proportion of the more spherical calcite particles and a higher percentage of vaterite was observed at higher copolymer concentrations.

Increasing the calcium concentration to 20 mM yielded a similar pattern of morphological changes as those observed at 10 mM with varying copolymer concentration (Figure 3). At a [Ca]:[S] molar ratio of 500:1, minor truncation of the rhombohedron corners and edges was observed (Figure 3a), an effect which became more pronounced at [Ca]:[S] = 250:1. Higher copolymer concentrations ([Ca]:[S] = 125:1) further enhanced this effect, producing larger truncations and particles with more rounded profiles (Figure 4b). The rounded form is a product of the larger truncations of the particle. In common with the results obtained at [Ca] = 10 mM, application of high copolymer concentrations induced a transformation in particle structure from single crystal to polycrystalline calcite with polycrystalline particles being produced at [Ca]:[S] $\approx$ 25:1 at 20 mM Ca (Figure 3c) compared to [Ca]:[S] $\approx$ 12.5:1 at 10 mM Ca (Figure 2e).

A marked difference in the mechanism of crystal growth was observed at lower calcium concentrations (1 mM [Ca]). In contrast to the single-crystal or spherical polycrystalline calcite particles observed at 10 or 20 mM Ca, polycrystalline particles with regular morphologies and planar faces were obtained for

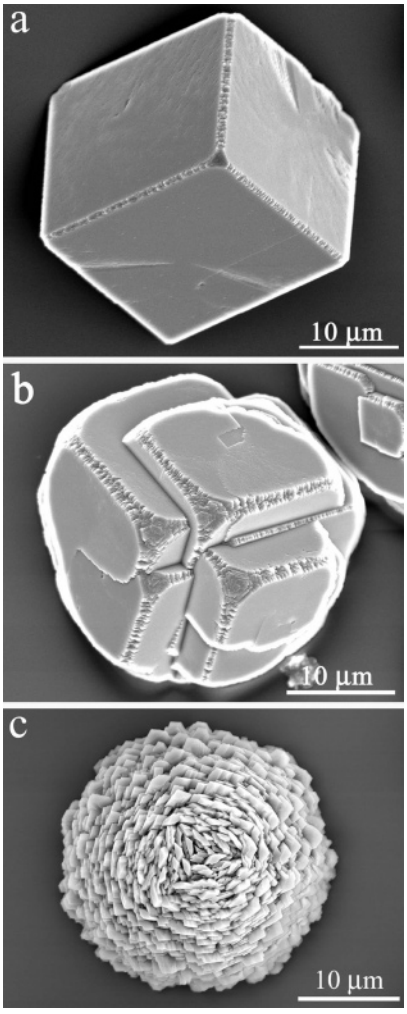

Figure 3. Calcium carbonate crystals precipitated from a solution containing 20 mM Ca and PEO_{22}-$PNaStS_{49}$ at a copolymer concentration such that the [Ca]:[S] molar ratio was (a) 500:1, (b) 125:1, and (c) 25:1. These crystals are representative of the entire sample population.

[Ca]:[S] molar ratios of 2.5:1 to 1:8. A typical particle morphology produced at a [Ca]:[S] molar ratio of 2.5:1 is shown in Figure 4a. In common with the morphological modifications observed at 10 and 20 mM Ca, this type of particle is based on edge and corner truncations of the basic rhombohedral form. Again, the majority of particles were oriented such that the [001] axis was approximately normal to the substrate. However, the defining characteristic of these particles is the roughness of their crystal faces, which contrasts markedly with the significantly smoother faces shown in Figure 3 for [Ca] = 20 mM. Examination of these faces at high magnification (Figure 4b) strongly suggests that the particles are constructed from small, distinct crystalline units. This hypothesis is supported by a BET specific surface area of 30 $m^2\ g^{-1}$, which is close to the value of 39 $m^2\ g^{-1}$ recorded for the polycrystalline particles produced in the presence of PEO_{22}-$PNaStS_{49}$ at [Ca] = 10 mM and a [Ca]:[S] molar ratio of 1.25:1. Despite their polycrystalline nature, these particles are highly oriented, as demonstrated by their uniform extinction along the *c* axis between crossed polars in an optical microscope. Calcite particles with such "mesocrystal" structures have been described previously by Cölfen et al. using poly(sodium 4-styrenesulfonate) homopolymer as an additive.[18,21] An interesting morphological modification, con-

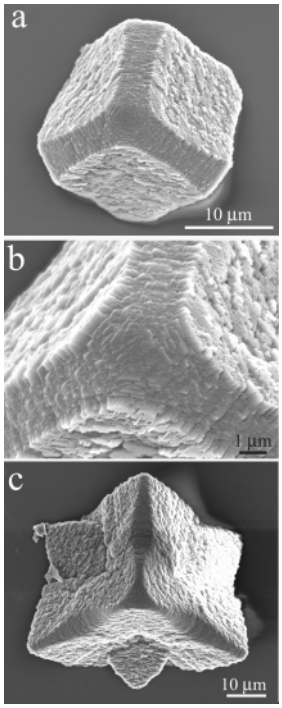

Figure 4. Calcium carbonate crystals precipitated from a solution containing 1 mM Ca and PEO_{22}-$PNaStS_{49}$ at a copolymer concentration such that the [Ca]:[S] molar ratio was (a) 2.5:1 and (b and c) 1.25:1. Image b shows details of the surface structure of a crystal produced at a [Ca]:[S] molar ratio of 1.25:1. These crystals are representative of the entire sample population (not shown).

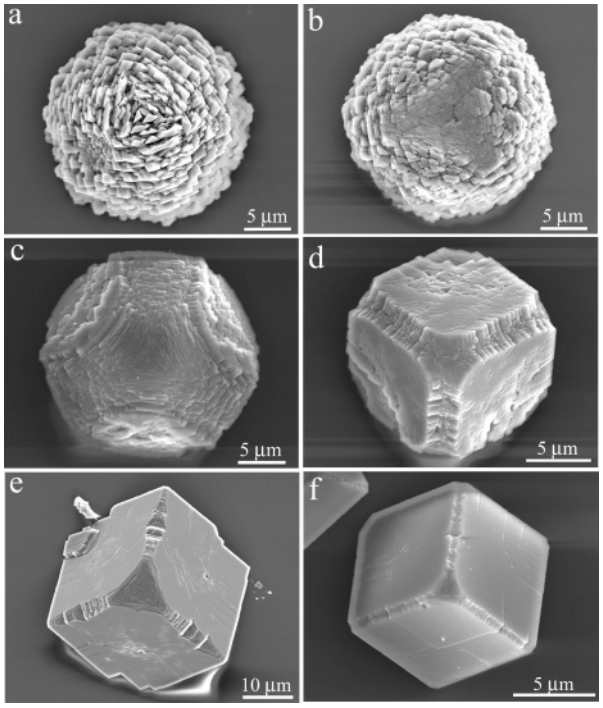

Figure 5. Calcium carbonate crystals precipitated from a solution containing Ca and PEO_{22}-$PNaStS_{49}$ at a fixed [Ca]:[S] molar ratio of 1.25:1 and Ca concentrations of (a) 10, (b) 5, (c) 2.5, (d) 1, (e) 0.5, and (f) 0.1 mM. These crystals are representative of the entire sample population.

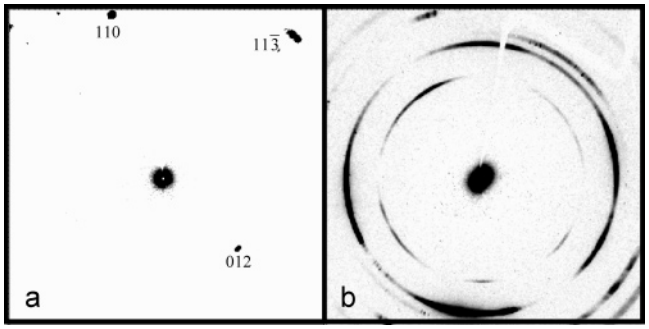

Figure 6. Selected microbeam diffraction patterns from single calcium carbonate particles precipitated from a solution containing Ca and PEO_{22}-$PNaStS_{49}$ at a fixed [Ca]:[S] molar ratio of 1.25:1 and Ca concentrations of (a) 2.5 (corresponding to Figure 6c) and (b) 10 mM (corresponding to Figure 6a). The reflections seen in a and b correspond to calcite.

sistent with twinning,[23] was also observed under similar reaction conditions (for [Ca]:[S] = 1.25:1) and is shown in Figure 4c. Here, triangular prismatic outgrowths occur on each of the {104} faces such that the 3-fold symmetry around the [001] axis is maintained. Further increasing the copolymer concentration did not have a significant effect on the particle morphology and ultimately inhibited crystal growth at a [Ca]:[S] molar ratio of ~1:6.

Due to the strong dependence of the particle structure and morphology on the calcium concentration, a series of experiments was performed to investigate the effect of the calcium-ion concentration at a constant [Ca]:[S] molar ratio of 1.25:1 (Figure 5). Within the range [Ca] = 10−0.1 mM, a continuous variation in structures was observed. Ca concentrations of 10 (Figure 5a) and 5 mM (Figure 5b) generated particles that were clearly polycrystalline in structure, although the emergence of a triangular top face is apparent at 5 mM. A Ca concentration of 2.5 mM (Figure 5c) results in a particle with marked 3-fold symmetry in which the constituent crystalline units are significantly smaller, leading to somewhat smoother surfaces. At a Ca concentration of 1 mM (Figure 5d), the particles have well-defined rhombohedral morphologies with significantly roughened faces, modified with the characteristic corner and edge truncations. Morphologies consistent with assignment of a single-crystal structure were observed at low Ca concentrations. Rhombohedral calcite particles with minor corner and edge truncations were produced at 0.5 (Figure 5e) and 0.1 mM (Figure 5f) Ca, with the particle faces produced at 0.1 mM being almost entirely smooth. This series of particles clearly demonstrates that no abrupt morphological transition occurs between single-crystal and polycrystalline structures but that a continuum of structures exists between these two extremes.

Two members of this morphological series of particles were also investigated with an X-ray microbeam of 15 μm diameter, giving diffraction patterns from individual particles. Diffraction patterns from several single particles were collected, and representative patterns are shown in Figure 6. These data provide considerable insight into the nanostructures of the particles. The [Ca] = 2.5 mM particle, despite showing a rounded profile and rough surfaces (Figure 5c), diffracts like a single crystal, showing only a few isolated spots in the diffraction pattern. It was not possible to carry out an orientational analysis as this would have required sample rotation. However, given that both the {006} and {104} reflections are fully missing, this indicates that the specimen normal is close to the [001] direction. The [Ca] = 10 mM particles (Figure 5a), in contrast, showed powder rings as expected for a polycrystalline assembly of small

(23) Dana, J. D. *The System of Mineralogy*, 7 ed.; J. Wiley and Sons: New York, 1951; Vol. 2.

crystallites. These diffraction rings, however, exhibited strong texturing, indicating a substantial degree of preferred orientation for these crystallites. The width of the reflections was also used to obtain an estimate of the lower limit for the crystallite size (Scherrer size) of the [Ca] = 10 mM particles of about 60−80 nm. The reflections from the [Ca] = 2.5 mM particles appear to be slightly narrower than those from the [Ca] = 10 mM particles but are too close to the resolution limit of the instrument to provide reliable crystallite sizes.

All particles also showed a strong SAXS signal close to the direct beam (Figure 6). The SAXS pattern is anisotropic for the [Ca] = 10 mM particles but more isotropic for the calcite particles in the [Ca] = 2.5 mM series. The azimuthally averaged SAXS profiles from the calcite particles produced under both conditions are similar in shape and consistent with scattering from plate-shaped nanoparticles. This result is consistent with the hypothesis of calcite mesocrystal evolution developed previously.[21] An estimate of the thickness D of these platelets, made by applying Guinier's law,[24] gives $D \approx 2.2$ nm for the 10 mM particles and $D \approx 3.7$ nm for the 2.5 mM particles These values are much lower than the estimated lower limit of the Scherrer size from the crystalline reflections and cannot therefore be attributed to the primary calcium carbonate crystallites. The SAXS signal may therefore tentatively be attributed to ultrathin polymer regions between or within the primary calcium carbonate crystallites which could arise from the original polymer coating on the nanoparticles, although porosity may also play a role.

Although the PEO_{45}-$(PGMA:2SBA)_{48}$ diblock copolymer also comprised an ionic block with pendent aromatic sulfonic acid groups, marked differences were observed for this copolymer in its mechanism of interaction with the growing calcium carbonate crystals. While systematic morphology modifications could be produced with this polymer, only single-crystal type morphologies were observed. The detailed experimental observations are described in the Supporting Information.

Thermogravimetric analyses (TGA) of selected samples were carried out to investigate the extent of copolymer incorporation within the calcite crystals. Single-crystal $CaCO_3$ particles grown in the presence of PEO_{45}-$(PGMA:2SBA)_{48}$ with [Ca] = 10 mM and [Ca]:[S] = 1:1 exhibited a 2% weight loss below 600 °C, indicating a relatively low level of copolymer incorporation. In contrast, the polycrystalline calcite aggregates grown using PEO_{22}-$PNaStS_{49}$ at [Ca] = 10 mM and [Ca]:[S] = 1.25:1 had a weight loss of 7.5%, while the mesocrystal particles formed with PEO_{22}-$PNaStS_{49}$ at [Ca] = 1 mM and [Ca]:[S] = 1.25:1 showed a 3.5% weight loss below 600 °C. In contrast, control calcite crystals precipitated in the absence of any copolymer additives exhibited negligible mass loss at comparable temperatures. The structure of the particles was also probed by BET surface area analysis to determine their effective surface area. Calcite crystals produced using PEO_{45}-$(PGMA:2SBA)_{48}$ with [Ca] = 10 mM and [Ca]:[S] = 1:1 had a BET surface area of 6 $m^2\ g^{-1}$, which is comparable to a value of 3.5 $m^2\ g^{-1}$ obtained for control calcite crystals. The polycrystalline particles produced in the presence of PEO_{22}-$PNaStS_{49}$ under identical conditions exhibited a significantly higher surface area of 39 $m^2\ g^{-1}$, while the mesocrystals produced with PEO_{22}-$PNaStS_{49}$ at [Ca] = 1 mM and [Ca]:[S] = 1.25:1 had a BET surface area of 30 $m^2\ g^{-1}$.

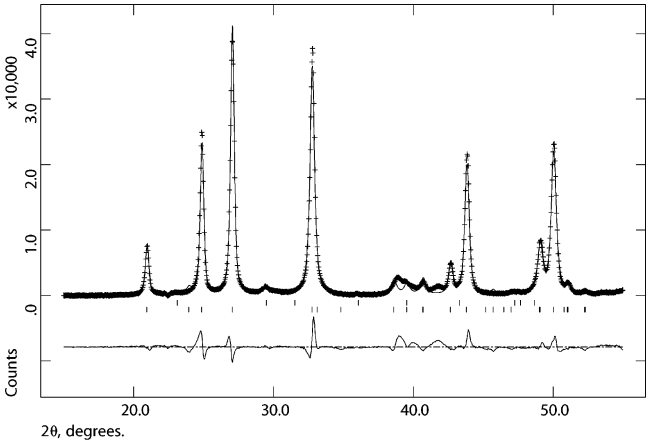

Figure 7. XRD pattern of the calcium carbonate particles produced using $PNaStS_{79}$. (+ + +) experimental data and (- - -) calculated fit for 4 wt % calcite, 96 wt % vaterite. The upper tick marks are the expected calcite peak positions; the lower refer to the vaterite. Note the unmodeled intensity at approximately $2\theta = 40°$.

Rietveld quantitative phase analysis of the powder XRD pattern for $CaCO_3$ produced with PEO_{22}-$PNaStS_{49}$ at [Ca] = 10 mM and [Ca]:[S] = 1.25:1 indicated that the inorganic phase comprised 45 wt % calcite and 55 wt % vaterite. A good fit is obtained to the calcite structure, while the vaterite phase can only be fitted to a significantly altered version of one of the three published structures for vaterite (space group *Pbnm*[25]) but not to any of the hexagonal structures (SI Table 1).[26,27] This significantly different structure was developed using an XRD pattern collected on a sample produced with $PNaStS_{79}$ that comprised 96 wt % vaterite and 4 wt % calcite. Further, the fit to this structure is imperfect (Figure 7), perhaps suggesting formation of another polymorph with a close structural relationship to that in ref 25. Indeed, Dupont et al.[28] also published vaterite XRD powder patterns which cannot be easily fitted to published vaterite structures but do not comment further on this issue. In contrast, the particles produced with the PEO_{45}-$(PGMA:2SBA)_{48}$ diblock copolymer at [Ca] = 10 mM and [Ca]:[S] = 1:1 have a powder pattern with peak positions that match the calcite lattice. However, this sample shows a single additional reflection at $d = 2.735$ Å (32.7° 2θ) and another much weaker one at $d = 2.236$ Å (40.3° 2θ). These additional reflections are in fact from vaterite, and the pattern of intensities from the calcite phase does not match well with that expected from calcite despite several attempts at modeling this with preferred orientation and other parameters. A control calcite sample was synthesized using a standard protocol,[29] and a Rietveld structural refinement gave an excellent match to the published structure (data not shown).

Discussion

The PEO_{22}-$PNaStS_{49}$ diblock copolymer is extremely versatile in that it produces a wide range of particle structures depending on the precise experimental conditions. According to traditional

(24) Glatter, O.; Kratky, O. *Small Angle X-ray Scattering*; Academic Press Inc. Ltd.: London, 1982.

(25) Meyer, H. J. *Fortsch. Mineral.* **1960**, *38*, 186−187.
(26) Kamhi, S. R. *Acta Crystallogr.* **1963**, *16*, 770−772.
(27) Meyer, H. J. *Z. Kristallogr.* **1969**, *128*, 183−212.
(28) Dupont, L.; Portemer, F.; Figlarz, M. *J. Mater. Chem.* **1997**, *7*, 797−800.
(29) Agarwal, P.; Berglund, K. A. *Cryst. Growth Des.* **2003**, *3*, 941−946.

and modern classifications, three principal classes of particle structures are observed, namely, single crystals, mesocrystals, and polycrystalline aggregates with some degree of orientation. The single-crystal regime is defined by well-facetted particles with predominantly smooth surfaces and single-crystal scattering behavior (as exemplified by the particles shown in Figure 5e and 5f). No nanoparticle building units can be recognized on the faces of these particles. Mesocrystals, on the other hand, as exemplified by the particles shown in Figures 4a and 5c, have rougher surfaces, porosity, and the primary nanoparticles from which these particles are constructed can often be recognized. They also show single-crystal scattering behavior, although some misalignments may become visible in the scattering pattern depending on the mutual orientation of the primary nanoparticles in the mesocrystal. Finally, polycrystalline aggregates are defined by little or no orientational order, porosity, and clearly visible nanoparticle subunits (Figure 5a).

The data presented here, however, suggest that such rigid classification of particle structures into single crystal, mesocrystal, and polycrystalline may be premature. Figure 5 shows that simply varying the Ca concentration at a fixed [Ca]:[S] molar ratio of 1.25:1 leads to a *continuous transition* from textured polycrystalline aggregates to mesocrystals to single-crystal structures on reducing the Ca and copolymer concentrations. This suggests that *no abrupt change* in the mechanism of particle formation occurs and thus that all of these structures are generated by aggregation-based routes. Indeed, this conclusion is supported by the observation that even the particles which appear morphologically as random polycrystalline aggregates (Figure 5a) possess a degree of preferred orientation. Lowering the solution concentrations of Ca and/or copolymer then results in a gradual increase in the degree of orientation, producing the mesocrystal particles. The most intriguing structures, however, are possibly the 'single-crystal' particles. By extending the above argument, the continuous transition in particle structures suggests that these 'single crystals' also form via an aggregation-based mechanism. On reducing the Ca and copolymer concentrations, the size of the precursor units would be expected to decrease until the limiting case of classical ion-by-ion growth is attained at low Ca and copolymer concentrations. Similar arguments were used to explain the change in structures and morphologies of calcite particles obtained in the presence of poly(acrylic acid).[30]

Growth of colloidal particles in solution is generally considered to occur either by coarsening of primary particles to produce single crystals or via aggregation processes.[31,32] Aggregation can in turn produce amorphous, polycrystalline, or single crystals, depending on the structure of the primary particles, whether the aggregation process is random or directional and whether recrystallization occurs after aggregation.[20,31,33,34] While formation of nonoriented polycrystalline particles is both common and easily identified, single-crystal formation via aggregation appears to be rather less common. However, it is likely that this mechanism operates more frequently than currently assumed as the final product morphology is often indistinguishable from a single crystal formed by ion-by-ion growth. Identification is therefore typically achieved through time-resolved analysis of the formation mechanism[35−37] or by analysis of the internal nanostructure of the particles,[18,38−40] which however only characterizes the final particles. Examples include formation of lenticular hematite particles via aggregation of nanometer-sized precursor particles,[41] prismatic copper oxalate,[42,43] dodecahedral $(NH_4)_3PW_{12}O_{40}$,[44] and others as reviewed in ref 20. Growth of nanoparticles by this mechanism has also been characterized in a wide range of systems including nanoparticle growth of TiO_2 (anatase), Fe_2O_3 (hematite), and CoO(OH) (heterogenite).[34,45]

Aggregation-based mechanisms can lead to formation of highly ordered particle assemblies by a number of routes. For example, hematite particles built from oriented nanoparticle blocks can form via random aggregation of oxyhydroxide precursor particles, followed by their recrystallization to give an ordered particle assembly, and subsequent dehydration to give hematite.[34,46] The precursor particles can also undergo oriented aggregation to form an ordered assembly prior to dehydration to give hematite.[34] Finally, hematite nanoparticles formed by dissolution and reprecipitation of precursor particles can directly undergo oriented aggregation.[34] The morphologies of the product particles can also provide insight into the precise mechanism, since a dissolution step should lead to isotropic particles, whereas oriented aggregation may be preferred along a given crystallographic direction and often generates final particle morphologies that reflect the morphology of the primary particles.

Directional aggregation can be driven by a number of processes. Removal of solvent or adsorbed molecules from selected particle surfaces and formation of new chemical bonds via epitaxial contacts act as a driving force for particle growth by oriented aggregation.[45] The existence of a net magnetic or electric dipole, which in the latter case can often develop as a result of adsorption of additives to specific faces of the primary particles, can also drive formation of product particles with atypical morphologies.[47] For example, copper oxalate mesocrystals were produced in the presence of hydroxypropylmethylcellulose (HPMC) with the final particles varying from cushion-like crystals precipitated in the absence of HPMC to cubic and ultimately rod-like mesocrystals at higher HPMC concentrations.[42] These particle morphologies were rationalized in terms of preferential adsorption of the HPMC onto the

(30) Donnet, M.; Bowen, P.; Jongen, N.; Lemaître, J.; Hofmann, H. *Langmuir* **2005**, *21*, 100−108.
(31) Penn, R. L. *J. Phys. Chem. B* **2004**, *108*, 12707−12712.
(32) Park, J.; Privman, V.; Matijevic, E. *J. Phys. Chem. B* **2001**, *105*, 11630−11635.
(33) Ocana, M.; Rodriguez-Clemente, R.; Serna, C. J. *Adv. Mater.* **1995**, *7*, 212−216.
(34) Penn, R. L.; Oskam, G.; Strathmann, T. J.; Searson, P. C.; Stone, A. T.; Veblen, D. T. *J. Phys. Chem. B* **2001**, *105*, 2177−2182.
(35) Testino, A.; Buscaglia, M. T.; Viviani, M.; Buscaglia, V.; Nanni, P. *J. Am. Ceram. Soc.* **2004**, *87*, 79−83.
(36) Testino, A.; Buscaglia, M. T.; Buscaglia, V.; Viviani, M.; Bottino, C.; Nanni, P. *Chem. Mater.* **2004**, *16*, 1536−1543.
(37) Testino, A.; Buscaglia, V.; Buscaglia, M. T.; Vivianni, M.; Nanni, P. *Chem. Mater.* **2005**, *17*, 5346−5356.
(38) Oaki, K.; Imai, H. *Angew. Chem., Int. Ed.* **2005**, *44*, 6571−6575.
(39) Simon, P.; Schwarz, U.; Kniep, R. *J. Mater. Chem.* **2005**, *15*, 4992−4996.
(40) Donnet, M.; Bowen, P.; Jongen, N.; Lemaître, J.; Hofmann, H. *Langmuir* **2005**, *21*, 100−108.
(41) Ocana, M.; Morales, M. P.; Serna, C. J. *J. Colloid Interface Sci.* **1995**, *171*, 85−91.
(42) Jongen, N.; Bowen, P.; Lemaître, J.; Valmalette, J.-C.; Hofmann, H. *J. Colloid Interface Sci.* **2000**, *226*, 189−198.
(43) Soare, L. C.; Bowen, P. L.; Lemaitre, J.; Hofmann, H. *J. Phys. Chem. B* **2006**, *110*, 17763−17771.
(44) Ito, T.; Song, I.; Inumaru, K.; Misono, M. *Chem. Lett.* **1997**, *8*, 727−728.
(45) Niederberger, M.; Cölfen, H. *Phys. Chem. Chem. Phys.* **2006**, *8*, 3271−3287.
(46) Banfield, J. F.; Welch, S. A.; Zhang, H.; Ebert, T. T.; Penn, R. L. *Science* **2000**, *289*, 751−754.
(47) Simon, P.; Zahn, D.; Lichte, H.; Kniep, R. *Angew. Chem., Int. Ed.* **2006**, *45*, 1911−1915.

hydrophobic ϵ terminating faces of the primary crystallites. This results in modification of the morphology of the primary crystallites, which is reflected in the sequence of morphological changes in the product particles. Ellipsoidal hematite particles were formed via oriented aggregation by forced hydrolysis in the presence of phosphate ions.[41] The phosphate ions were believed to adsorb on the hematite primary particles on planes parallel to the *c* axis, resulting in an anisotropic morphology. Subsequent aggregation occurred preferentially along the *c* axis, possibly due to the magnetic properties of the hematite particles. This was accompanied by desorption of the phosphate ions, and sintering of the primary particles resulted in monocrystalline particles. Similarly, the oriented assembly of two spherical ZnO precursor particles along their *c* axes, which led to product particles with rod-like morphology, was postulated to be driven by the net polarization of the precursor particles along the *c* axis.[48]

Oriented aggregation to produce final particles with "mesocrystal structures" is most likely to occur if (1) the supersaturation is sufficiently high for the crystallization pathway to be shifted to a kinetic mechanism based on precursor nanoparticles,[49] (2) the primary particles are less concentrated in solution, allowing aggregation to occur under more ideal conditions compared to the random aggregation that occurs at high nanoparticle concentrations, and (3) the primary particles display well-defined morphologies. Thus, there are many examples of gel-grown mesocrystals formed through oriented aggregation since the gel viscosity minimizes random interactions between the primary particles.[50,51] That we observe a continuous transition from textured polycrystalline aggregate, through mesocrystal, to truncated single crystal on lowering the reagent concentrations at [Ca]:[S] = 1.25:1 is therefore consistent with these arguments. At higher concentrations the polycrystalline particles are formed from relatively large, morphologically well-defined crystallites (Figure 5a). On decreasing the concentration, mesocrystals are produced that are accompanied by a reduction in the size of the crystallites forming the product particles (Figure 5c and d). As the concentration is reduced yet further, the mechanism approaches a classical crystallization route where the product crystal develops via ion-by-ion growth.

The prevalence of [001] oriented particles and the characteristic pattern of edge and corner truncations are intriguing. The {001} face of calcite is either purely anionic or cationic and therefore only exhibited on stabilization, typically through adsorption of an additive. The anionic sulfonated copolymers PEO_{22}-$PNaStS_{49}$ and PEO_{45}-$(PGMA{:}2SBA)_{48}$ examined in this study are clearly suitable candidates for stabilization of a cationic {001} face; adsorption of copolymer on the substrate prior to particle formation may well direct the final [001] orientation of the product particles. The way in which the polymer adsorbs to the substrate is not known, but PNaStS[18,21] and oligoethyleneoxide units[52] have been reported to induce a [001] orientation of calcite on glass. Predominantly [001] oriented calcite has also been grown on sulfonated polystyrene films[53] and under Langmuir monolayers of *n*-eicosyl sulfate and *n*-eicosyl phosphonate.[54] Selection of the {001} face was generally considered on the basis of nonspecific electrostatic interactions, although in the case of the Langmuir monolayers, stereochemical recognition between the monolayer headgroup and nucleating crystal was suggested as the primary factor in determining crystal orientation.

In contrast to the PEO_{22}-$PNaStS_{49}$ diblock copolymer, PEO_{45}-$(PGMA{:}2SBA)_{48}$ only produced single-crystal-type particles over a wide range of experimental conditions. This fundamental difference in behavior must derive from differences in the mode of interaction of the polymers with the surfaces of the calcite primary particles and also with Ca ions in solution. The single-crystal particles exhibited characteristic edge and corner truncations, the sizes of which varied according the experimental conditions. SI Figure 2 shows particles precipitated in the presence of PEO_{45}-$(PGMA{:}2SBA)_{48}$ diblock copolymer, which typically have a very large truncated top face and well-defined rhombohedral morphologies. While the pattern of single-crystal truncations found for calcite crystals grown in the presence of PEO_{45}-$(PGMA{:}2SBA)_{48}$ is similar to that obtained with PEO_{22}-$PNaStS_{49}$, the former copolymer produces much larger corner truncations while maintaining a very well-defined rhombohedral morphology and relatively smooth faces. It therefore appears that the PEO_{45}-$(PGMA{:}2SBA)_{48}$ copolymer mediates a highly ordered aggregation process.

Our proposed model of calcium carbonate crystallization in the presence of copolymer additives is summarized in Figure 8, which shows how the product particle structure develops as a function of the calcium and polymer concentrations in solution. Polycrystalline particles form at the highest supersaturations, where rapid nucleation generates a large number of precursor nanoparticles. Adsorption of copolymer molecules to the surfaces of the nanoparticles can modify their morphologies and significantly limits their growth such that growth by aggregation of these stabilized nanoparticles proceeds more rapidly than coarsening of the individual nanoparticles. Once aggregated, the nanoparticles are held together by van der Waals forces, and only limited orientation or reorientation can occur to give polycrystalline particles with either no or a low degree of orientational ordering. In addition, a large amount of polymer (7.5 wt % from TGA data) is occluded within the polycrystalline particles, remaining as a 2−3 nm layer (SAXS) around the calcite nanoparticles in the aggregate. Trapping of the polymer within the particles is again a direct result of the rapid aggregation process.

Reduction in the supersaturation to a level where primary nanoparticles are still formed in solution but at low enough concentrations to enable oriented aggregation yields mesocrystals. The polymer additive again modifies the size and shape of the primary nanoparticles, and the smaller number of particles produced at the lower supersaturation leads to slower aggregation. Under these conditions, oriented aggregation and movement of the nanoparticle subunits within the aggregates can occur to bring them into crystallographic register, a process which is

(48) Verges, M. A.; Mifsud, A.; Serna, C. J. *J. Chem. Soc., Faraday Trans.* **1990**, *86*, 959−963.
(49) Ma, Y. R.; Cölfen, H.; Antonietti, M. *J. Phys. Chem. B* **2006**, *110*, 10822−10828.
(50) Busch, S.; Dolhaine, H.; DuChesne, A.; Heinz, S.; Hochrein, O.; Laeri, F.; Podebrad, O.; Vietze, U.; Weiland, T.; Kniep, R. *Eur. J. Inorg. Chem.* **1999**, *10*, 1643−1653.
(51) Grassmann, O.; Neder, R. B.; Putnis, A.; Löbmann, P. *Am. Mineral.* **2003**, *88*, 647−652.
(52) Popescu, D. C.; Leeuwen, E. N. M. v.; Rossi, N. A. A.; Holder, S. J.; Jansen, J. A.; Sommerdijk, N. A. J. M. *Angew. Chem., Int. Ed.* **2006**, *45*.
(53) Addadi, L.; Moradian, J.; Shay, E.; Maroudis, N. G.; Weiner, S. *Proc. Natl. Acad. Sci.* **1987**, *84*, 2732−2736.
(54) Heywood, B. R.; Mann, S. *Chem. Mater.* **1994**, *6*.

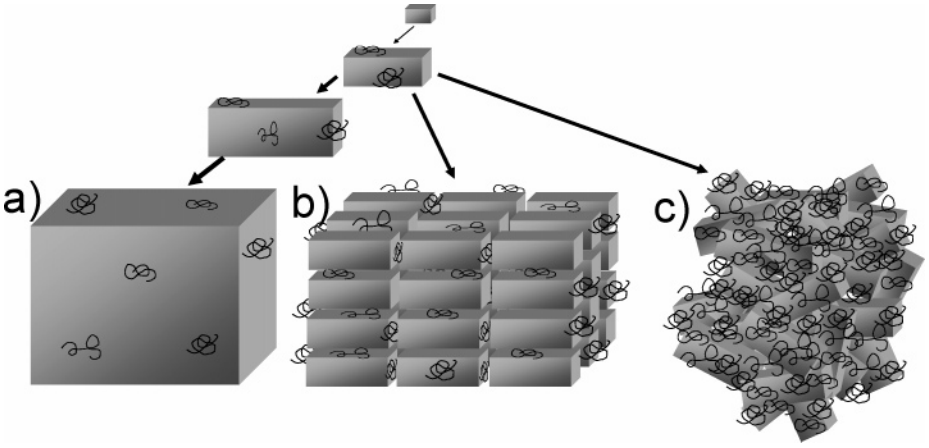

Figure 8. Unifying crystallization mechanism including (a) classical ion/molecule-mediated crystallization, amplifying a critical crystal nucleus to a single crystal and (b and c) nonclassical particle-based crystallization pathways leading to a mesocrystal (b) or polycrystal (c). The choice of the crystallization pathway depends on additives like copolymers, which retard particle growth and thus lead to particle aggregation-based crystallization mechanisms. A continuum of structures between a and c is possible.

accompanied by rearrangement or desorption of the polymer. This is reflected in the lower polymer content of the mesocrystals (3.5 wt % from TGA) as compared with the polycrystalline particles.

Finally, single crystals form at low supersaturations, where the primary units in solution are small clusters, molecules, and ions. Growth can then occur by oriented aggregation of these clusters or classical ion-by-ion addition to nascent nuclei and is accompanied by adsorption of the polymer additive onto selected crystal faces, resulting in morphological control. This reduction in subunit size is also anticipated to be accompanied by a significant decrease in the quantity of polymer encapsulated within the particles. The polymer will associate much more weakly with small clusters and be readily displaced during aggregation/crystallization to give the single-crystal product particles.

Such a common crystallization framework allows for the observed continuous transition between the different product morphologies. The polycrystalline and mesocrystal particles are both constructed from copolymer-stabilized nanoparticle subunits with the transition between these structures simply deriving from the degree of orientation of the precursor nanoparticles in the final crystal. Although perhaps less obvious, we also show that a continuous transition also occurs between the mesocrystal and single-crystal structures. The transition between particle-mediated nonclassical crystallization and ion-by-ion-based classical crystallization is also not sharp and purely based on the size of the units building up the crystal. Indeed, a continuous range of intermediates between ions and nanoparticles can be imagined, including clusters, oligomers, and complexes. Additionally, the nanoparticle subunits in a mesocrystal are already in crystallographic register and can fuse to give either a continuous single crystal in the ideal case or an intermediate structure.

This description of additive-controlled crystallization is therefore entirely continuous, suggesting that the crystallization pathways to polycrystalline, mesocrystal, and single-crystal product particles, which had previously been considered to be distinct, all form part of a unified crystallization framework. Indeed, a brief review of the literature fully supports our hypothesis that single-crystal growth via oriented aggregation may be *at least* as common as the classical picture of ion-by-ion growth. Further, we observed that clearly polycrystalline mesocrystals scatter like a single crystal (Figure 6a)—even if rotated in three dimensions.[49] It is therefore essential that the distinction between a single crystal, mesocrystal, and polycrystal be made on the basis of the crystallographic perfection of the solid and its single crystal/polycrystalline morphology rather than on the mechanism by which it formed.[55]

Conclusions

This work presents strong support for a unifying model of copolymer-directed crystallization, demonstrating experimentally for the first time that a continuous transition in particle structures and crystallization mechanisms occurs between polycrystalline aggregates, mesocrystals, and single crystals. We suggest that all of these particle structures can occur via aggregation processes and that the mode of aggregation varies from a low to a high degree of orientation, with a reduction in the solution supersaturation. Further, at sufficiently low supersaturation levels the mechanism approaches classical ion-by-ion growth and single crystals form whose morphologies are dictated by polymer adsorption onto selected crystal faces.[49] In conclusion, our results show that it is necessary to view additive-controlled crystallization in a much broader context than has been considered previously and that growth of single crystals via classical ion-by-ion growth, particle-mediated oriented aggregation leading to mesocrystals or nonoriented aggregation yielding polycrystalline particles are all parts of a common crystallization framework.

Acknowledgment. Financial support of A.N.K. from the Engineering and Physical Sciences Research Council (EPSRC, grant GR/S79732/01) is gratefully acknowledged. H.C. and O.P. acknowledge financial support from the Max-Planck Society. S.P.A. is the recipient of a 5-year Royal Society Wolfson Research Merit Award. EPSRC is thanked for support of Y.L. through a Platform Grant (GR/S25845), and we would additionally like to thank Dr. C. D. Vo for assistance with polymer synthesis.

Supporting Information Available: Experimental methods used and a description of $CaCO_3$ crystallization in the presence of PEO_{45}-$(PGMA:2SBA)_{48}$. This material is available free of charge via the Internet at http://pubs.acs.org.

JA067422E

(55) Towe, K. M. *Biomineralization Forschungsberichte* **1972**, *4*, 1−14.